

CHARACTERIZATION OF A SYNCHRONOUS WAVE NONLINEAR TRANSMISSION LINE

P. D. Coleman^{*}, J. J. Borchardt, J. A. Alexander, J. T. Williams, T. F. Peters

Sandia National Laboratories, P.O. Box 5800, MS 1153

Albuquerque, NM 87185, USA

Abstract

Many aspects of Non Linear Transmission Lines (NLTL's) make them attractive sources for High Power Microwave (HPM) systems. This paper describes a test bed that is being used to investigate synchronous wave NLTL operations.

Analytical models and numerical simulations are used in design of the line and interpretation of results. Shock wave propagation is characterized and compared to theoretical predictions.

Adjustment of the shock velocity is used to demonstrate the NLTL's tunability. Forward wave operation of the line has been fully characterized using fast shock velocities. In addition, backward wave operation has been observed when using slow shock velocities.

I. INTRODUCTION

Nonlinear transmission lines (NLTL's) are seen as attractive alternatives to vacuum devices in generating high power microwaves. The lines require no vacuum systems and avoid x-ray production associated with high energy electrons in vacuum. Electronic biasing of the line's magnetic or dielectric materials allows frequency agility that is not easily obtained in many high power vacuum oscillators. In addition, the NLTL's construction can be made more mechanically rugged than typical vacuum devices.

Three forms of NLTL's have been discussed in the literature: gyromagnetic oscillators [1, 2], soliton generators [3, 4, 5, 6, 7], and synchronous wave generators [8, 9, 10].

Katayev [11] has a comprehensive summary of shock wave propagation on ferrite loaded lines. Combining this shock propagation with a dispersive line leads to the potential for synchronous wave generation. Much theoretical work has been done looking at the physics of synchronous wave generation [8, 9]. These lines have been shown to have both forward and backward wave modes of operation [12, 13, 14].

In this paper, we use a moderate power test bed to investigate the various modes of operation for a synchronous wave NLTL. The paper is organized by first

reviewing synchronous wave theory. This is followed by a description of the testbed used to characterize the NLTL. Experimental results of shock propagation are next presented and compared to theory. Finally, RF wave evolution, tuning, and power measurements are presented.

II. THEORY

A. Principle of Operation

The figure below shows an equivalent circuit used in modeling the NLTL.

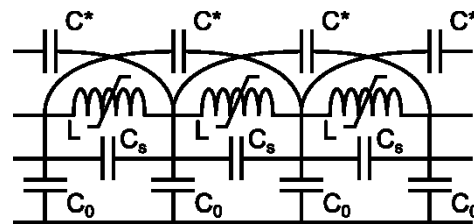


Figure 1. Equivalent circuit used in modeling the NLTL.

The basic line consist of the ladder network formed by the ferrite loaded inductors L and the primary capacitors C₀. The coupling capacitors C^{*} are used to modify the RF wave dispersion in such a way as to optimize the pulse shape generated [9]. C_s represents parasitic capacitance shunting the primary inductors.

A high amplitude pulse is injected into the line. This injected pulse drives the ferrites into saturation and forms a shock front. Behind the shock front a linear dispersive transmission line is formed by the lumped capacitances, C₀, and saturated inductors, L₀. Energy from the shock front then couples to RF waves that have phase velocities matching the shock velocity, v_s (i.e. synchronous wave).

Operation of the NLTL can be analyzed from two perspectives: shockwave propagation and the RF wave propagation. The next sections detail these two aspects of the line's operation.

B. Shock Wave Propagation

The normalized shock velocity can be expressed as [8]:

$$v_s = \left[1 + \frac{(1 - m_0) \cdot \eta \cdot M/p}{I_s} \right]^{-1/2} \quad (1)$$

^{*} email: pdcolem@sandia.gov

Here, m_0 is the initial magnetization, M is the saturation magnetization, η is the ferrite filling factor, p is a geometric factor for scaling current to magnetic field, and I_s is the shock current. Note that the shock velocity is a function of both drive level, I_s and the initial magnetization (see Shock Propagation Curves section).

C. RF Wave Propagation

For saturated conditions, the dispersion relation for the circuit shown in Fig. 1 is given by

$$\alpha^2 = \frac{\sin^2(\varphi/2)}{1 + 4 \cdot \delta \cdot \sin^2(\varphi/2) + 4 \cdot \gamma \cdot \sin^2\varphi} \quad (2)$$

Where $\alpha = \omega/\omega_c$, $\omega_c = 1/\sqrt{L_0 C_0}$, ω is the RF angular frequency, φ is the phase shift per unit cell, $C^* = \gamma \cdot C_0$, and $C_s = \delta \cdot C_0$. Note that in the limit of $C_s=0$ this reduces to Belyantsev's dispersion relation [8].

Structures with this type dispersion relation can support both forward and backward wave modes of operation [12]. This paper focuses on characterizing the forward mode of operation (RF phase and group velocities in the same direction). However, limited backward wave operation (RF phase and group velocities in opposite directions) has also been observed.

D. Numerical Modeling

The circuit shown above in Fig. 1 can be used to model the NLTL's performance [8, 9]. Kirchoff voltage and current equations are coupled with the Landau-Lifshitz-Gilbert equation [15] which models the nonlinear magnetic components in the line.

Each section yields equations relating voltage, current and magnetization resulting in approximately 3N coupled 1st order ordinary differential equations to solve. A MATLAB Runge-Kutta routine is used to solve the set of equations.

III. EXPERIMENTAL RESULTS

The experimental layout is shown in the figure below.

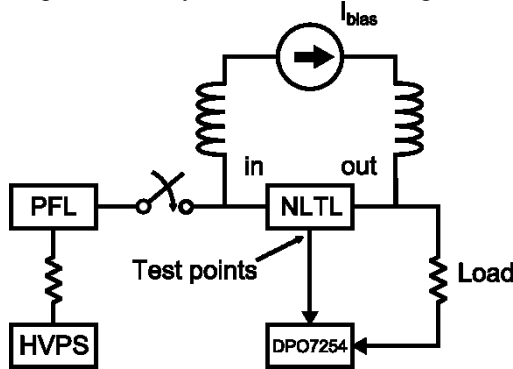


Figure 2. Block diagram of experimental setup.

A high voltage power supply is used to charge an external modulator (Pulse Forming Line, PFL, cable pulser). Once charged, the switch closes launching a 100 ns, 10 – 40 kV pulse into the NLTL. A 0-10A, inductively isolated, bias supply is used to set the ferrites' initial magnetization. A Tektronix DPO 7254 2.5 GHz scope monitors the NLTL's output along with test points distributed down the line.

A. Line Description

A 200 segment line was constructed and housed in a 2 m long, 2"x1" extruded Al tube (see Fig. 3). Yttrium Iron Garnet, YIG, ($B_{sat}=1780$ G, $B_r=1280$ G) was used for the nonlinear ferrite.



Figure 3. Photograph of the 200 segment NLTL experimental hardware.

HFSS, ANSYS's 3D full-wave electromagnetic simulation, was used to model RF propagation on the physical line. In this case, the ferrites are assumed to be saturated, and therefore no shockwave propagation physics is included. However, this tool has been very useful in modeling RF propagation on the constructed hardware. The Fig. 4 shows HFSS's calculated dispersion relation for this structure.

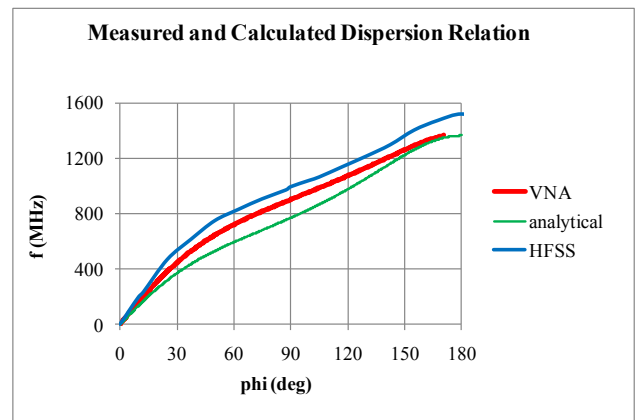


Figure 4. Structure's dispersion relation: red – VNA measured, green – analytical prediction, blue – HFSS calculation.

A Vector Network Analyzer, VNA, was used to measure the dispersion relation for the line. In order to simulate a fully saturated ferrite condition, the ferrites were removed from the structure for the sweep. The resultant curve is plotted in the figure above for comparison to the HFSS calculation.

Also plotted are predictions from the analytic expression in Eq. 2. A 3D electrostatic solver is used to estimate values for C_0 , C_s , and C^* . L_0 is then derived by fitting the curve at f_{max} . All three curves have similar forms, with HFSS slightly overestimating the frequency and the analytical model slightly underestimating the frequency.

B. Shock Propagation Curves

The shock velocity was measured by monitoring V-dots located at stage 2 and 200 on the line. A dc bias current is used to set the initial magnetization of the ferrite. The plot below shows the shock velocity for a fixed PFL charge as the initial magnetization is varied.

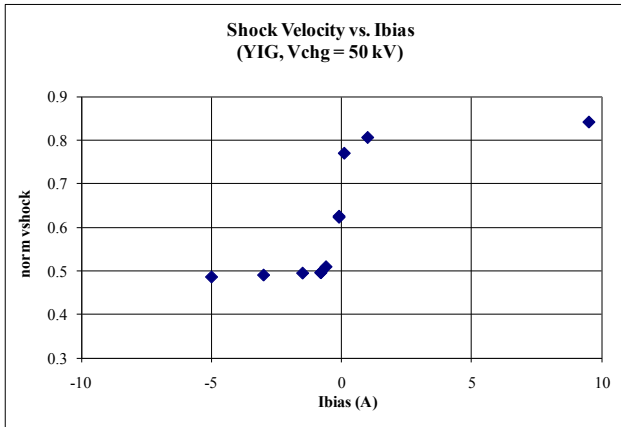


Figure 5. Measured normalized shock velocities as a function of applied bias current (PFL charge voltage held constant).

The velocity is seen to be a strong function of the bias current. This dependence is key to the NLTL's tunability (see RF Results section).

The shock velocity was also measured as a function drive level. The plot below shows a comparison between measured velocities and that predicted by Eq. 1.

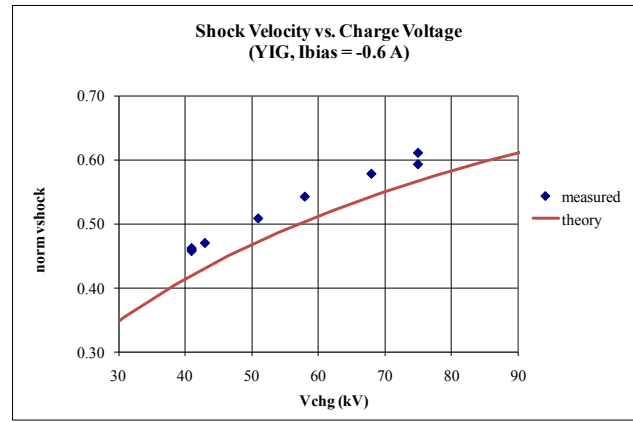


Figure 6. Measured and predicted shock velocities as function of PFL's charge voltage (initial magnetization held constant).

The theory predicts the measured velocities to within 10%. The agreement gives one confidence in the shock propagation portion of the NLTL operation.

C. RF Results

Three aspects of the measured RF generation are summarized below: Wave evolution, tuning, and power vs frequency.

1) Wave evolution

The numerical model was used to predict expected results for forward wave operation. Simulated waveforms for different points along the line are shown in the figure below.

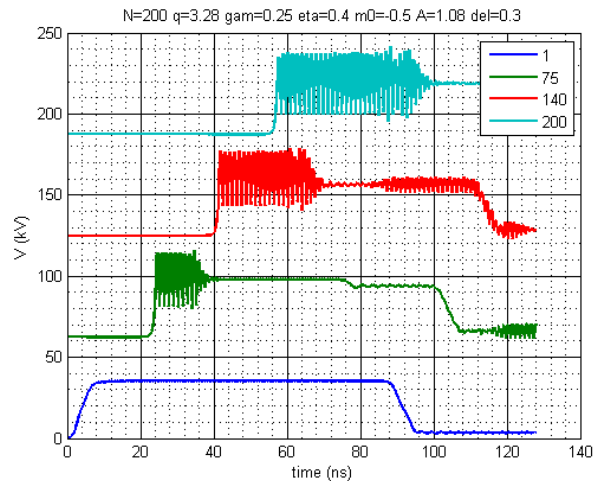


Figure 7. Numerical model predictions for waveforms at segments 1, 75, 140, and 200.

Note, that for this forward wave mode, the model predicts the pulsewidth to increase as the shock front moves down the line.

Experimentally, the RF propagation was monitored using capacitive V-dot probes placed along the NLTL. The outputs from V-dots located at segments 2, 75 and 200 are displayed below.

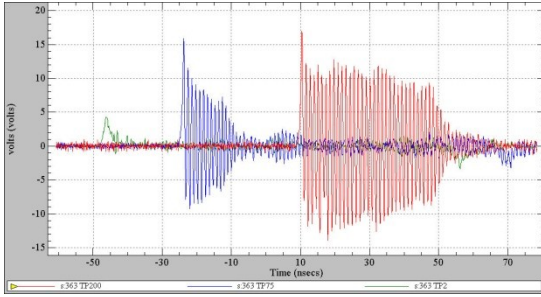


Figure 8. Measured V-dot waveforms at segments 2 (green), 75 (blue), and 200 (red).

The measured data show the number of oscillations growing, as predicted, as the shock front propagates down the line.

2) Tuning curve

The NLTL couples energy from the shock front to an RF wave whose phase velocity matches the shock velocity. Hence there is a direct relationship between frequency and shock velocity.

A convenient form to illustrate the tunability of the NLTL is to plot the frequency vs. normalized shock velocity (or equivalently normalized phase velocity). An overlay of the predicted tuning curve (based on VNA measurements) along with measured data is shown below.

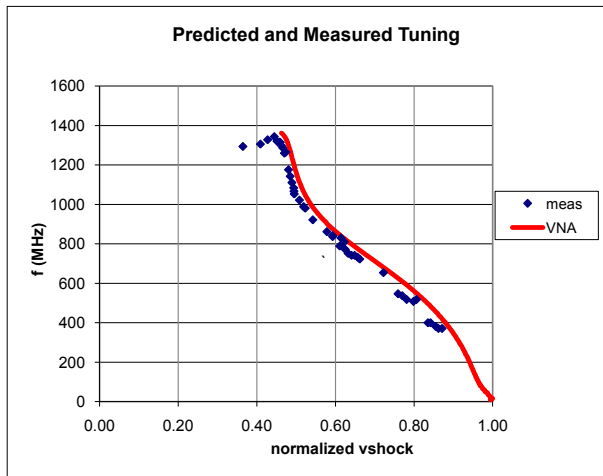


Figure 9. Predicted and measured tuning results. Red is tuning predicted from VNA measurements. Blue is measured frequencies from NLTL shots.

In this case the shock velocity was varied by adjusting the drive amplitude and initial magnetization. The generated power is far from constant over this range;

however, the agreement seen above is a strong indication of synchronous wave operation for the NLTL.

Note that the drop in frequency observed at velocities less than 0.45 corresponds to backward wave operation. In this case RF was present at the input end of the line as opposed to the output for forward wave operation.

3) Power vs. Frequency

To study the line's output power vs frequency, the PFL's charge voltage was fixed and the frequency varied by adjusting m_0 . The plot below is the result of that scan.

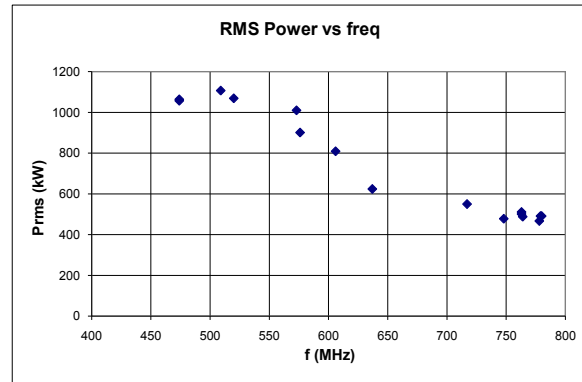


Figure 10. RMS output power at different operating frequencies.

The measured powers are well under (a factor of 6 – 9) that predicted by the lossless numerical model. This discrepancy is most likely due to non-ideal ferrite material properties. Results of characterizing the YIG in a coaxial shock line geometry indicate that risetimes of 1.5 ns are achieved for the typical NLTL drive levels. This may limit the frequency content available for converting into higher frequency RF. RF losses in the ferrite and resistive losses in the conductors, will undoubtedly also lead to lower RF levels.

IV. SUMMARY

This paper has described the design, modeling and operation of a ferrite loaded synchronous wave NLTL. Forward wave operation has been thoroughly characterized and evidence of backward wave operation has also been observed. Good agreement is observed between shock propagation measurements and models. Measured RF tuning and wave evolution also agree well with the numerical model. However, extracted powers fall well short of the lossless model prediction (probably due to non-ideal ferrite material properties).

V. ACKNOWLEDGEMENTS

The authors would like to thank Sandia's Compact Pulsed Power team for providing technical support of the experimental effort. This work was funded by Sandia National Laboratories' Laboratory Directed Research and Development program.

VI. REFERENCES

- [1] J. E. Dolan, "Simulation of shock waves in ferrite-loaded coaxial transmission lines with axial bias," *J. Phys. D: Appl. Phys.*, vol. 32, pp. 1826-1831, 1999.
- [2] J. Bragg, J. Dickens, A. Neuber, "Magnetic Biasing of Ferrite Filled Nonlinear Transmission Lines," *Proceedings 2010 IEEE International Power Modulator and High Voltage Conference*.
- [3] H. Ikezi, S. S. Wojtowicz, R. E. Waltz, J. S. DeGrassie, and D. R. Baker, "High-power soliton generation at microwave frequencies," *J. Appl. Phys.*, vol. 64 (6), pp. 3277-3281, 1988.
- [4] H. Ikezi, J. S. DeGrassie, and J. Drake, "Soliton generation at 10 MW level in the very high frequency band," *Appl. Phys. Lett.*, vol. 58 (9), pp. 986-987, 1991.
- [5] P. Brown, PhD. Thesis, University of Oxford, 1997.
- [6] Q. R. Marksteiner, B. E. Carlsten and S. Russell, "Numerical calculations of RF efficiency from a soliton generating nonlinear transmission line", *J. Appl. Phys.*, vol. 106 (11), p. 113306, 2009.
- [7] Q. R. Marksteiner, B. E. Carlsten and S. Russell, "Efficient Generation of RF using a Biased Soliton Generating Nonlinear Transmission Line with a Bipolar Input", *Micro. Opt. Techn. Lett.*, vol. 52 (6), p. 1411, 2010.
- [8] A. M. Belyantsev, A. I. Dubnev, S. L. Klimin, Yu. A. Kobelev, and L. A. Ostrovskii, "Generation of radio pulses by an electromagnetic shock wave in a ferrite-loaded transmission line," *Tech. Phys.*, vol. 40 (8), pp. 820-826, 1995.
- [9] A. M. Belyantsev and A. B. Kozyrev, "Influence of local dispersion on transient processes accompanying the generation of rf radiation by an electromagnetic shock wave," *Tech. Phys.*, vol. 43 (1), pp. 80-85, 1998.
- [10] N. Seddon, C. R. Spikings and J. E. Dolan, "RF pulse formation in nonlinear transmission lines," *Proceedings 2007 IEEE Pulsed Power Conference, 2007*, p. 678.
- [11] I. G. Katayev, *Electromagnetic Shock Waves*, Illife, London, 1963.
- [12] A. M. Belyantsev and A. B. Kozyrev, "Generation of RF oscillations in the interaction of an electromagnetic shock with a synchronous backward wave," *Tech. Phys.*, vol. 45 (6), pp. 747-752, 2000.
- [13] N. Seddon and T. Bearpark, "Observation of the Inverse Doppler Effect," *SCIENCE*, vol. 302, pp. 1537-1540, 2003
- [14] A. B. Kozyrev and D. W. van der Weide, "Explanation of the inverse Doppler effect observed in nonlinear transmission lines," *Phys. Rev. Lett.*, vol. 94, p. 203902, 2005.
- [15] E. M. Gyorgy, "Rotational model of flux reversal in square loop ferrites," *J. Appl. Phys.*, vol. 18 (9), pp. 1011-1015, 1957.